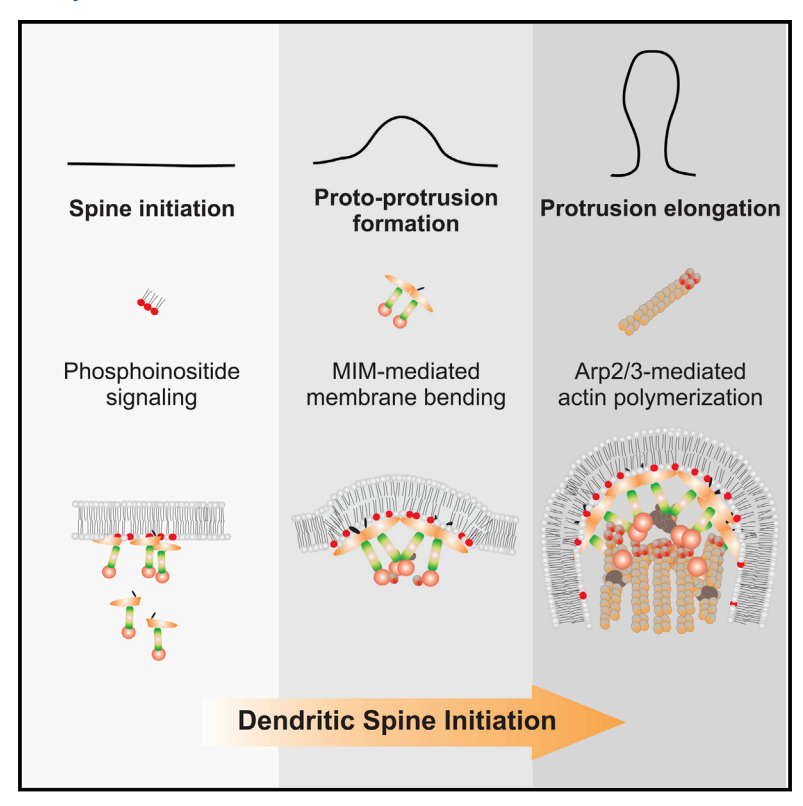
Developmental Cell

MIM-Induced Membrane Bending Promotes Dendritic Spine Initiation

Graphical Abstract



Authors

Juha Saarikangas, Nazim Kourdougli, Yosuke Senju, ..., Pekka Lappalainen, Claudio Rivera, Pirta Hotulainen

Correspondence

juha.saarikangas@bc.biol.ethz.ch (J.S.), claudio.rivera@helsinki.fi (C.R.), pirta.hotulainen@helsinki.fi (P.H.)

In Brief

Saarikangas et al. describe how direct membrane bending by inverse-BAR protein MIM/MTSS1 generates protoprotrusions, promoting subsequent actin assembly and leading to the initiation of dendritic spines in neurons. MIM deficiency results in defective spine formation, abnormal synaptic transmission, and corresponding behavioral defects in mice.

Highlights

- MIM deforms plasma membrane into proto-protrusions that initiate spine formation
- PIP₂ promotes MIM recruitment and subsequent Arp2/3mediated actin assembly
- MIM deficiency decreases and overexpression of MIM increases spine density
- Loss of MIM in mice results in aberrant synaptic transmission and behavior



Developmental Cell





MIM-Induced Membrane Bending Promotes Dendritic Spine Initiation

Juha Saarikangas,^{1,2,*} Nazim Kourdougli,³ Yosuke Senju,¹ Genevieve Chazal,³ Mikael Segerstråle,⁴ Rimante Minkeviciene,⁵ Jaakko Kuurne,⁵ Pieta K. Mattila,^{1,16} Lillian Garrett,⁶ Sabine M. Hölter,^{6,7} Lore Becker,^{8,9} Ildikó Racz,¹⁰ Wolfgang Hans,⁸ Thomas Klopstock,^{9,11} Wolfgang Wurst,^{6,7,12,13} Andreas Zimmer,¹⁰ Helmut Fuchs,⁸ Valérie Gailus-Durner,⁸ Martin Hrabě de Angelis,^{8,11,12,14} Lotta von Ossowski,⁴ Tomi Taira,¹⁵ Pekka Lappalainen,¹ Claudio Rivera, 3,5,* and Pirta Hotulainen 5,*

SUMMARY

Proper morphogenesis of neuronal dendritic spines is essential for the formation of functional synaptic networks. However, it is not known how spines are initiated. Here, we identify the inverse-BAR (I-BAR) protein MIM/MTSS1 as a nucleator of dendritic spines. MIM accumulated to future spine initiation sites in a PIP₂-dependent manner and deformed the plasma membrane outward into a proto-protrusion via its I-BAR domain. Unexpectedly, the initial protrusion formation did not involve actin polymerization. However, PIP2-dependent activation of Arp2/3-mediated actin assembly was required for protrusion elongation. Overexpression of MIM increased the density of dendritic protrusions and suppressed spine maturation. In contrast, MIM deficiency led to decreased density of dendritic protrusions and larger spine heads. Moreover, MIM-deficient mice displayed altered glutamatergic synaptic transmission and compatible behavioral defects. Collectively, our data identify an important morphogenetic pathway, which initiates spine protrusions by coupling phosphoinositide signaling, direct membrane bending, and actin assembly to ensure proper synaptogenesis.

INTRODUCTION

Precise control of the development and connectivity of synapses is critical for accurate neural network activities that control the regulation of organismal physiology and behavior (Alvarez and Sabatini, 2007; Bourne and Harris, 2008). The majority of the post-synaptic terminals of excitatory synapses reside in dendritic spines. Spines develop from filopodia-like precursors (thin actin-filled membrane protrusions) that mature into more variable morphologies, typically being characterized by a bulbous head and a narrow neck. Spines are highly dynamic and may undergo structural remodeling in response to changes in pattern and strength of neuronal activity (Alvarez and Sabatini, 2007; Bourne and Harris, 2008). Importantly, the capacity to undergo morphological remodeling and adopt a defined shape is considered to be a key step in determining the individualization and function of a given spine, implying the need for highly elaborate mechanisms that control spinogenesis and the plasticity of spines (Bourne and Harris, 2008). The actin cytoskeleton is known to play a pivotal role in the morphogenesis of dendritic spines (reviewed in Hotulainen and Hoogenraad, 2010; Svitkina et al., 2010). However, the mechanism of spine initiation at the dendritic plasma membrane has remained elusive.

One important group of proteins that function at the interface between plasma membrane and actin dynamics is the inverse-BAR (I-BAR) domain-containing proteins. In contrast to

¹Institute of Biotechnology, P.O. Box 56, University of Helsinki, 00014 Helsinki, Finland

²Institute of Biochemistry, ETH Zurich, 8093 Zurich, Switzerland

³Université de la Méditerranée, UMR S901 Aix-Marseille 2, Institut de Neurobiologie de la Méditerranée, 13009 Marseille, France

⁴Department of Biosciences, P.O. Box 56, University of Helsinki, 00014 Helsinki, Finland

⁵Neuroscience Center, P.O. Box 56, University of Helsinki, 00014 Helsinki, Finland

⁶German Mouse Clinic, Institute of Developmental Genetics, Helmholtz Zentrum München, German Research Center for Environmental Health (GmbH), 85764 Neuherberg, Germany

⁷Chair of Developmental Genetics, Technische Universität München c/o Helmholtz Zentrum München, German Research Center for Environmental Health (GmbH), 85764 Neuherberg, Germany

⁸German Mouse Clinic, Institute of Experimental Genetics, Helmholtz Zentrum München, German Research Center for Environmental Health (GmbH), 85764 Neuherberg, Germany

⁹Department of Neurology, Friedrich-Baur-Institut, Ludwig-Maximilians-Universität München, 80336 Munich, Germany

¹⁰Institute of Molecular Psychiatry, University of Bonn, 53105 Bonn, Germany

¹¹German Center for Vertigo and Balance Disorders, University Hospital Munich, 81377 Munich, Germany

¹²German Center for Neurodegenerative Diseases, 80336 Munich, Germany

¹³Max-Planck-Institute of Psychiatry, 80804 Munich, Germany

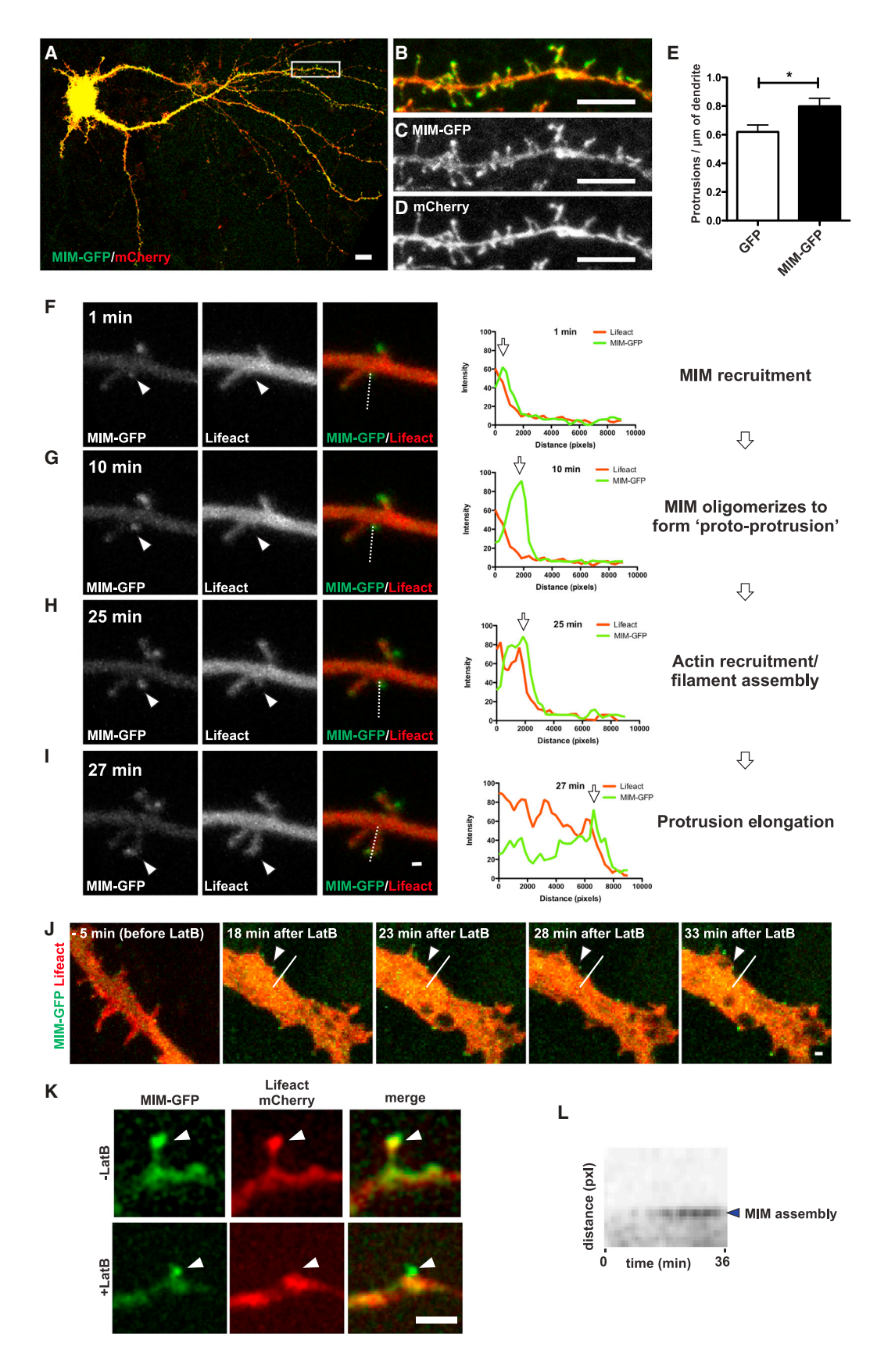
¹⁴Chair of Experimental Genetics, Center of Life and Food Sciences Weihenstephan, Technische Universität München, 85350 Freising-Weihenstephan, Germany

¹⁵Faculty of Veterinary Medicine, P.O. Box 56, University of Helsinki, 00014 Helsinki, Finland

¹⁶Present address: Institute of Biomedicine, University of Turku, 20520 Turku, Finland

^{*}Correspondence: juha.saarikangas@bc.biol.ethz.ch (J.S.), claudio.rivera@helsinki.fi (C.R.), pirta.hotulainen@helsinki.fi (P.H.) http://dx.doi.org/10.1016/j.devcel.2015.04.014







canonical BAR proteins, the I-BAR and inverse-F-BAR (IF-BAR) proteins bend the plasma membrane outward, promoting the formation of actin-rich cell protrusions (Zhao et al., 2011). Several I-BAR and IF-BAR proteins have been linked to many aspects of CNS function, including spine morphogenesis and neuronal migration (Carlson et al., 2011; Choi et al., 2005; Kim et al., 2009; Sawallisch et al., 2009; Guerrier et al., 2009; Charrier et al., 2012; Dharmalingam et al., 2009). Missing-in-metastasis (MIM/MTSS1) is among the CNS-expressed I-BAR proteins and is shown to deform membranes and bind to actin monomers (Mattila et al., 2003, 2007; Hayn-Leichsenring et al., 2011). MIM is conserved in metazoans and is important for proper kidney function and B cell development in mice (Saarikangas et al., 2011; Yu et al., 2012). However, neither the physiological role nor the molecular function of MIM in the CNS has been reported.

Here we provide evidence that MIM is a bona fide dendritic spine initiation factor. We show that phosphoinositide (PIP) signaling directs MIM to the plasma membrane where it bends the membrane to initiate dendritic filopodia formation. This initiation process is coupled to subsequent activation of PIPresponsive Arp2/3-mediated actin polymerization. Loss of MIM in mice results in decreased spine density in vitro and in vivo, whereas ectopic expression of MIM potentiates dendritic spine density and negatively regulates spine maturation. Finally, we demonstrate that MIM-deficient mice display attenuated excitatory synaptic transmission in the Purkinje cells and suffer from a complex set of behavioral defects, correlating with the morphological and functional manifestations found in the brain. Together, these data suggest that direct membrane deformation by membrane sculpting proteins might be a general mechanism to initiate cell protrusions.

RESULTS

MIM Forms Proto-Protrusions at Future Spine Assembly Sites Independently of Actin Assembly

To elucidate the molecular function of MIM in the CNS, we first examined the subcellular localization and function of MIM-GFP in 14 days in vitro (DIV) cultured rat primary neurons. Interestingly, MIM-GFP displayed a dendritic localization, preferentially accumulating to spine heads and dendritic filopodia (Figures 1A-1D). Comparison of the number of spines (density) in neurons expressing moderate levels of either GFP or MIM-GFP revealed that mild MIM overexpression significantly increased spine density (Figure 1E; p < 0.05). This suggested that MIM might play a role in spine initiation and/or stability. To test this further and to distinguish between these two options, we examined the spatiotemporal localization of MIM during spine formation. Curiously, we found that MIM-GFP signal often accumulated to dendrites at sites where the spine would be launched (arrowheads in Figures 1F-1I). Surprisingly, this accumulation occurred prior to actin assembly (Figure 1G), indicating that MIM is one of the first factors to mark the spine initiation site. Importantly, MIM accumulation resulted in the formation of a small proto-protrusion, to which actin then rapidly accumulated (compare Figures 1G and 1H). This subsequent actin accumulation resulted in a rapid elongation of a filopodial protrusion at the tip of which MIM was enriched (Figures 1G-1I).

Since it seemed that MIM alone was sufficient to initiate the protrusive activity at the future spine site (Figure 1G), it was important to confirm that the recruitment of MIM to the spine initiation sites and the subsequent formation of proto-protrusions were independent of actin polymerization. Therefore, we treated cells with latrunculin B (LatB), a drug that sequesters actin monomers thereby preventing filament assembly. Intriguingly, time-lapse imaging of cells treated with LatB showed that MIM continued to form small foci on the plasma membrane even in the absence of actin polymerization (Figures 1J and S1A). These MIM foci represented tiny proto-protrusions, typically less than 200 nm in length, without detectable F-actin accumulation (arrowhead in Figure 1K). Importantly, time-lapse imaging and kymograph analysis demonstrated that the MIM assembly in proto-protrusions was stable over several minutes, yet unable to elongate in the absence of actin filament assembly (Figures 1L, S1A, and S1B). Together, these findings indicate that MIM initiates the formation of spine proto-protrusions, which then recruit and promote actin assembly that drives the elongation of newly assembled spines.

MIM Displays a Neuron-Specific Distribution in the **Hippocampus and Cerebellum**

To gain a comprehensive understanding where MIM functions in the CNS, we examined the expression of MIM mRNA during CNS development by in situ hybridization of tissue sections. During embryonic days 14–18, MIM is strongly expressed in the cortical and neocortical regions (Figures 2A and 2B), indicating that MIM is a highly expressed gene during CNS development. We also performed an extensive immunohistochemical analysis with anti-MIM antibody (described in Hayn-Leichsenring et al., 2011) to identify the cell types that express MIM in the adult brain. This antibody recognized a single band of \sim 110 kDa from WT but not MIM^{-/-} cortical brain lysate on a western blot (Figure S2A). In agreement with the in situ hybridization results (Figure 2C), anti-MIM antibody labeled strongly cell bodies and dendrites of Purkinje cells, whereas no labeling was detected in the internal granular layer marked by NeuN (Figures 2D-2F). Importantly, no staining was detected with anti-MIM antibody in MIM knockout slices (Figure 2G). Since the CNS expression

Figure 1. MIM Initiates Dendritic Spine Formation prior to Actin Polymerization

(A-D) Rat hippocampal neuron transfected with mCherry and MIM-GFP.

- (E) Ectopic expression of MIM significantly increases the amount of dendritic spines (p < 0.05, Student's t test). Data are represented as mean ± SEM.
- (F-I) Time frames and line scans from the indicated regions of MIM and F-actin (Lifeact-RFP) dynamics during initiation of dendritic filopodia.
- (J) Time frames of MIM-GFP and Lifeact-RFP-transfected hippocampal neuron upon treatment with 5 µM LatB. In the absence of actin polymerization, MIM continues to accumulate at the membrane to form tiny proto-protrusions that are unable to elongate.
- (K) MIM dots observed in LatB-treated cells represent tiny protrusions that lack notable F-actin accumulation.
- (L) A kymograph analysis from the indicated region (white line in J) demonstrating that MIM proto-protrusions persist at the membrane over several minutes. Scale bars represent (A) 10 μ m, (B–D) 5 μ m, and (F–K) 1 μ m. See also Figure S1.



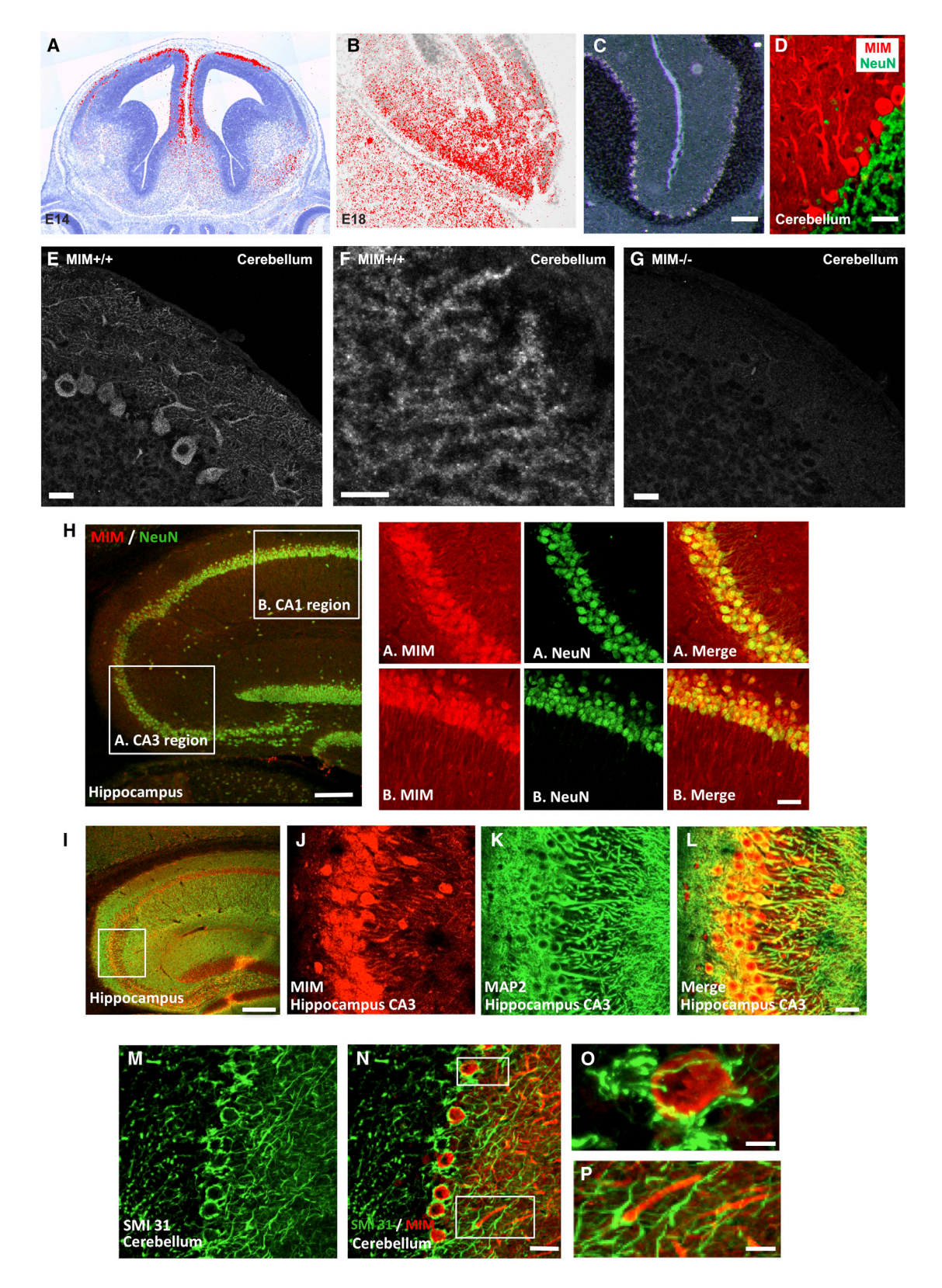


Figure 2. MIM Is Widely Expressed in the Developing and Adult CNS

(A and B) During brain development (E14–E18), MIM mRNA is detected in the cortex and the cortical plate at E14 and spreads to neocortical regions at E18. (C) In the adult brain MIM mRNA is expressed in cerebellar Purkinje cells.

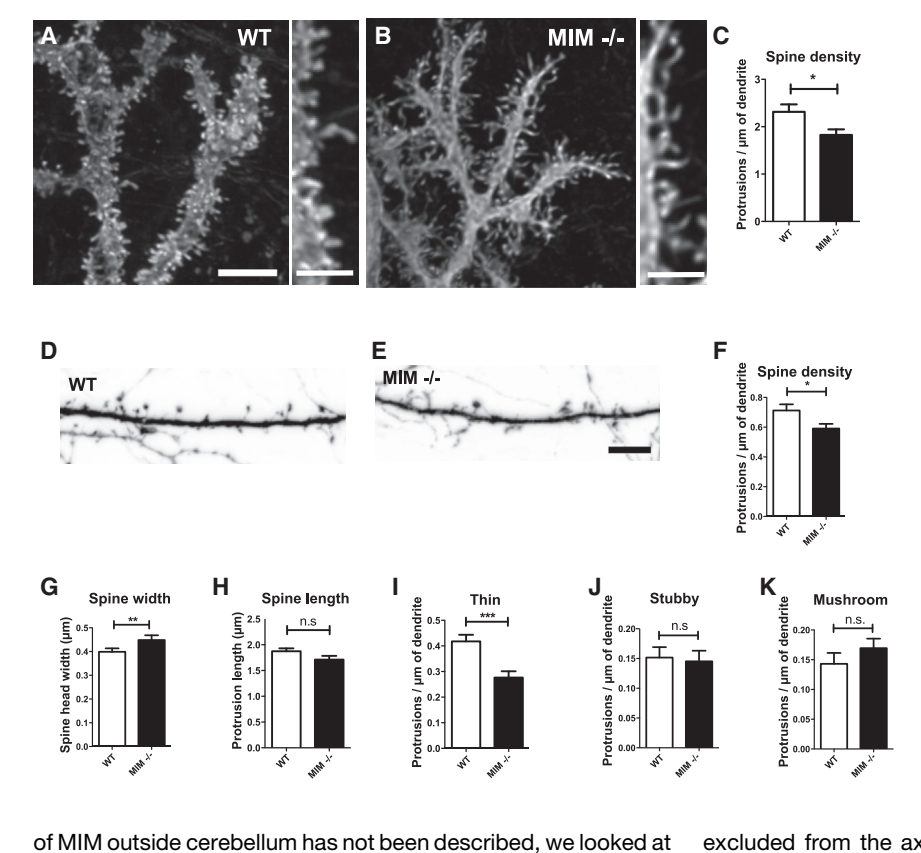


Figure 3. Loss of MIM Results in Reduced **Number of Dendritic Spines**

(A and B) Examples of biocytin injected Purkinje cells in the WT (A) and $MIM^{-/-}$ (B) cerebellar slices. (C) MIM^{-/-} Purkinje cell dendrites display a significant reduction in dendritic spine density as compared with WT mice ($MIM^{+/+}$: 2.31 ± 0.11 . SEM; $MIM^{-/-}$: 1.83 ± 0.16 SEM; p < 0.02, n = 13-15 per genotype).

(D and E) Representative images of dendrites of cortical neurons derived from MIM+/+ (D) and $MIM^{-/-}$ (E) mice.

(F-K) NeuronStudio analysis shows that the spine density, type distribution, and spine parameters differ between $MIM^{+/+}$ and $MIM^{-/-}$ neurons. MIM^{-/-} neurons had significantly decreased spine density (F, p < 0.05); especially the number of thin spines was reduced (I, p < 0.001). No significant changes were detected in the density of stubby or mushroom spines (J and K). The spine heads were wider in $\emph{MIM}^{-/-}$ than in WT neurons (G, p < 0.01). Data are represented as mean ± SEM. Scale bars represent 5 μm.

ure S2C). We conclude that MIM is expressed in the neuronal cells of the cortical and hippocampal regions of the cerebrum and in the Purkinje cells of the cerebellum. Importantly, MIM is

excluded from the axons, implying that it carries out dendrite specific functions in neurons.

MIM Deficiency Leads to Decreased Spine Density In Vivo and In Vitro

Since MIM displayed prominent localization to dendrites in different types of neurons and seemed to have a role in spine initiation, we wanted to test whether MIM deficiency leads to morphological abnormalities in dendritic spines in vivo. Thus, we analyzed the dendritic spine density in cerebellar Purkinje neurons, which express vast amount of MIM (Figures 2C and 2D). To compare spine densities between WT and MIM-deficient mice, we used biocytin-injected Purkinje neurons imaged with confocal microscopy and analyzed by NeuronStudio software (Figures 3A and 3B; data not shown). Importantly, we found a significantly decreased density of spines in MIM-/- mice as compared with the WT controls (Figure 3C; p < 0.05). This significant difference was also verified in an independent experiment using Golgi-stained Purkinje cells (data not shown).

Because detailed analysis of the exact spine morphology is difficult to perform in tissue slices, we made a more

hippocampus to find that NeuN positive pyramidal cells (CA1 and CA3) and granule cells (dentate gyrus) were immunopositive for MIM, displaying clear co-localization between NeuN and MIM

in the cell bodies (Figure 2H). To confirm MIM localization to den-

drites, we conducted a co-localization analysis with MIM and the

somato-dendritic marker MAP2. This showed a dendrite-spe-

cific localization in hippocampal pyramidal CA1 and CA3 cells

with high staining intensity in the proximal apical dendrites (Fig-

ure 21). Notably, co-staining of MIM with the axonal marker

SMI31 showed that MIM does not localize to axons in the cere-

bellar Purkinje cells, the pinceau formation (Figure 2J) or in the

hippocampal cell layers of the CA3, CA1 regions, or dentate

gyrus derived mossy fibers (Figure S2B; data not shown). More-

over, GFAP-positive glial cells were not detected with MIM antibody (data not shown), indicating that MIM is preferentially

expressed in neurons. Finally, we looked at cultured hippocam-

pal neurons and found that MIM antibody localized to discrete

foci along the dendritic shaft, reminiscent of the proto-protru-

sions/initiating filopodia (compare Figures 1F, S2C, and S2D),

but also of filopodia and occasionally in mature spines (Fig-

⁽D and E) The MIM protein is strongly detectable in Purkinje cell bodies and dendritic arborizations (red in D). No MIM labeling is visible in the NeuN-positive internal granular laver (green in D).

⁽F) Higher magnification of the area of (E) Purkinje cell dendrites reveals spiny staining pattern.

⁽G) Similar region as in (F) but from MIM^{-/-} cerebellum shows no staining with MIM antibody.

⁽H) In the hippocampus, the pyramidal layers are MIM positive. (H_A) Higher magnification of the CA3 pyramidal cells double labeled by NeuN and MIM. (H_R) CA1 pyramidal cells are NeuN and MIM immunopositive.

⁽I-L) MIM co-localizes with the dendritic marker MAP2 in hippocampal CA3 region pyramidal cells.

⁽M-P) MIM does not co-localize with the axonal marker SMI31 in cerebellum.

Scale bars represent (D, F, E H_A, H_B, and J-L) 20 µm, (C) 50 µm, (H and I) 200 µm, (J-L), (N and O) 10 µm, and (G) 5 µm. See also Figure S2.



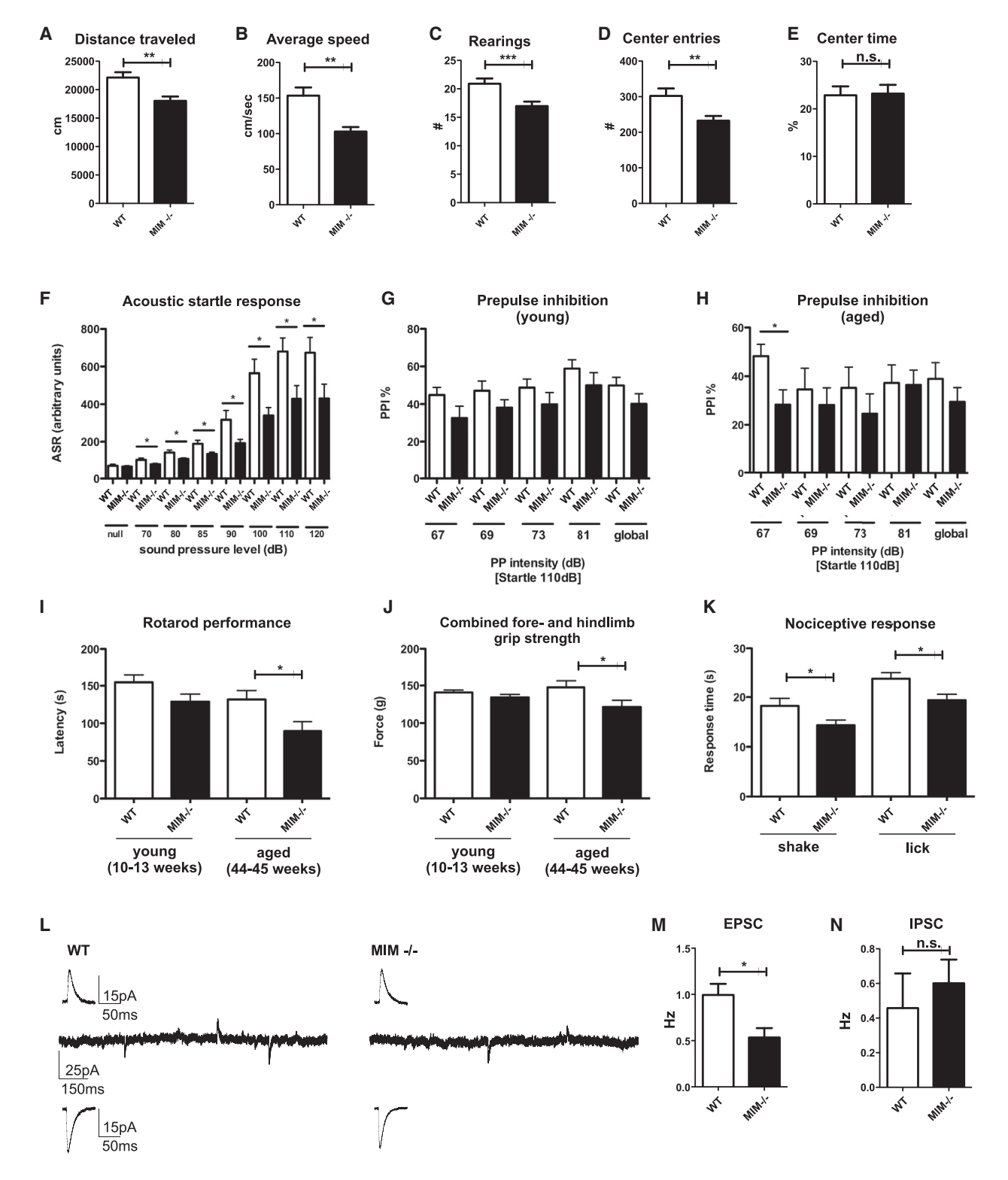


Figure 4. MIM Deficiency Leads to Altered Synaptic Transmission and Behavioral Abnormalities in Mice

(A–E) Open Field Test: 12- to 13-week old MIM mutants move less distance in the Open Field than WT controls (A), display reduced average speed (B), less rearing (C), and enter the center of the Open Field less frequently (D) than controls, but spend the same amount of time in the center (E). (F–J) MIM mutants display sensorimotor gating and motor coordination defects. (F) The ASRs were significantly reduced in 12- to 13-week-old MIM mutant mice. (G and H) The PPI was significantly reduced in aged (44–45 weeks old) mutant mice at low sound pressure intensity (67 dB) (H) with an overall reduced response trend in both young (G, 10–13 weeks) and aged (H, 44–45 weeks) mice. (I and J) $MIM^{-/-}$ mice display reduced performance in an accelerating rotarod and combined forelimb and hindlimb grip strength test, and the phenotype is more pronounced in aged 44- to 45-week-old mice.



comprehensive analysis on cortical (including hippocampal) neurons dissected from MIM-/- and WT littermates (Figures 3D and 3E). After 13 DIV, the neurons were transfected with GFP, and 1 day later (DIV14), the neurons were fixed and imaged by confocal microscope and spine density, and morphology was analyzed by NeuronStudio software (Rodriguez et al., 2008). Importantly, spine density was significantly decreased in cultured MIM^{-/-} hippocampal neurons (Figure 3F; p < 0.05), mirroring the phenotype of decreased spine density observed in Purkinje neurons in cerebellar slices. Morphological analysis of different spine types (Figures 3G-3K) showed that especially the number of thin spines was significantly reduced in MIM-/neurons (Figure 3I; p < 0.001). Moreover, the spine heads were wider in MIM-/- neurons as compared with WT neurons (Figure 3G; p < 0.01). Collectively, these data show that spine density is significantly reduced in MIM^{-/-} neurons both in vitro and in cerebellar tissues. The specific reduction found in the amount of thin spines is particularly interesting since thin spines (including dendritic filopodia) are the dynamic precursor structures of other spine types (Bourne and Harris, 2008). Thereby, loss of thin spines in the absence of MIM might reflect a defective initiation phase of spines, in line with the function of MIM during spine initiation (see Figure 1).

MIM Deficiency Leads to Defective Synaptic Transmission and Behavioral Abnormalities in Mice

The observed morphological alterations (Figure 3) urged us to subject the MIM mutant and control mice to a comprehensive set of behavioral tests to assess emotional, exploratory, and spontaneous locomotor behavior, sensorimotor gating, motor coordination, and nociceptive responses (http://www. mouseclinic.de; Gailus-Durner et al., 2009). Importantly, the behavioral analyses revealed significant differences between WT and their $MIM^{-/-}$ littermates. The open field test with 10to 11-week-old mice showed a significant reduction of exploratory activity in MIM^{-/-} mice. MIM knockout mice traveled in total less distance than controls (Figure 4A; p < 0.01), moved on average with a slower speed (Figure 4B; p < 0.01), exhibited reduced rearing frequencies (Figure 4C; p < 0.001), and entered the center of the Open Field less frequently than controls (Figure 4D; p < 0.01). This was due to significantly reduced total distance traveled in the periphery, since the time spent in the center did not differ from controls in young mice (Figure 4E).

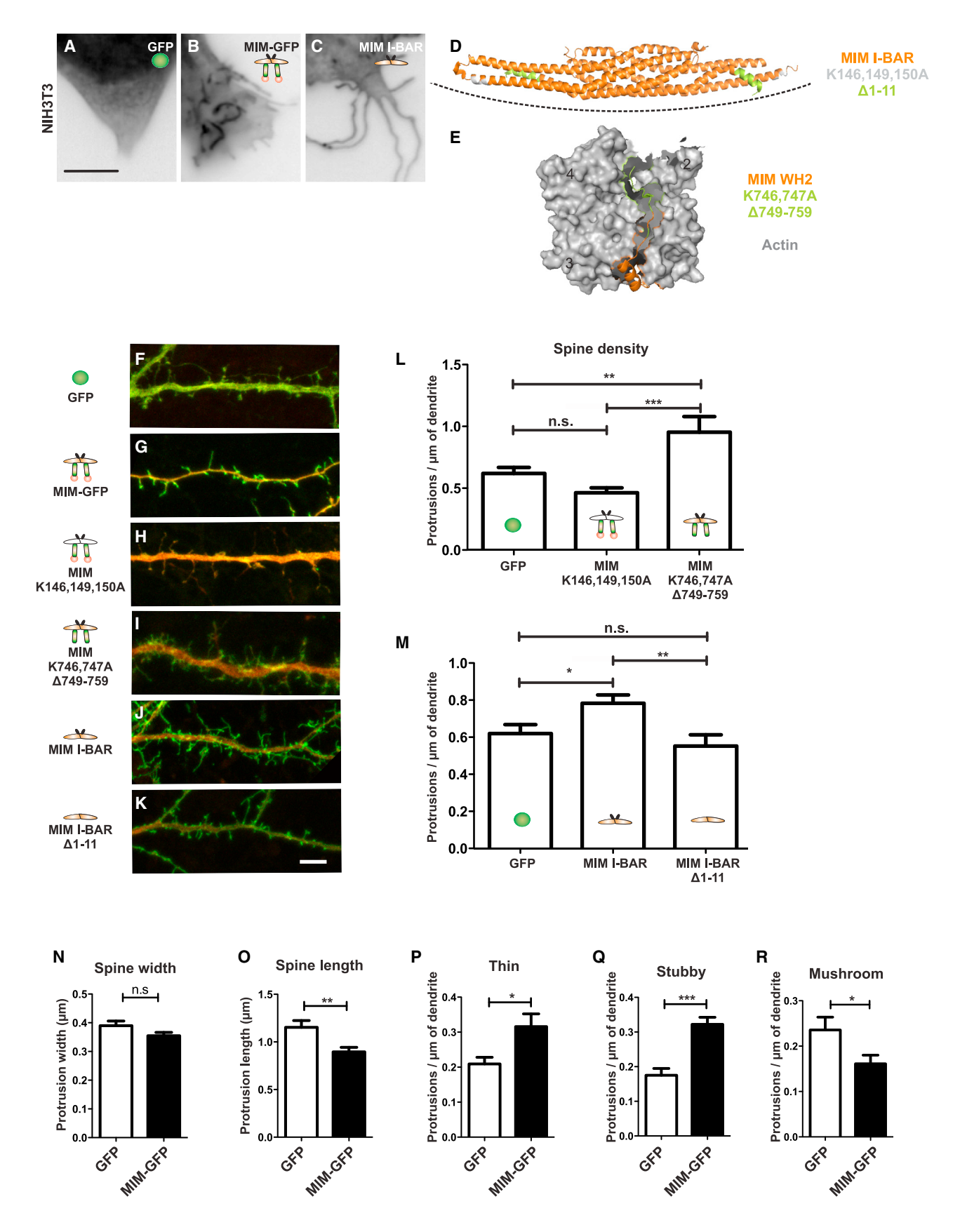
The high expression of MIM in cerebellum and the morphological anomalies detected in the Purkinje neurons of MIM-deficient mice prompted us to analyze the functionality of sensorimotor and coordination skills of MIM^{-/-} mice. Analysis of 12- to 13week-old mice revealed that MIM mutants had lowered acoustic startle responses (ASRs) as compared with control mice, especially at higher sound pressure levels (Figure 4F). Importantly, the clickbox test revealed no differences in the hearing capacities between WT and MIM-/- (data not shown), suggesting that the lowered ASR response of MIM-deficient mice originates from the CNS. To test the sensorimotor gating in $MIM^{-/-}$ mice, we employed Prepulse Inhibition (PPI) test. The 12- to 13week-old MIM^{-/-} mice showed overall lowered responses, albeit these were not statistically significant (Figure 4G). However, at the age of 44–45 weeks, there was a significant genotype effect of reduced PPI in mutants at 67 dB (Figure 4H; p < 0.05). To assess the coordination of MIM-/- mice, we used a Rotarod Test, which like PPI, revealed a decline in performance of MIM^{-/-} mice that was more pronounced in aged mice (Figure 4I; p < 0.05). A similar age-dependent decline in performance was also observed when we measured the Grip Strength (Figure 4J; p < 0.05). Finally, we analyzed the responsiveness of the somatosensory system to thermal pain in MIM mutant mice by a Hot Plate Test (nociceptive pain). Interestingly, MIM^{-/-} mice showed a hyperalgesic phenotype; i.e., the mutant mice reacted to thermal pain significantly faster as compared with WT mice (Figure 4K; p < 0.05). Together, these results show that MIM deficiency leads to a variety of behavioral defects, in agreement with the broad expression of MIM in different brain regions (Figure 2). We find it unlikely that the locomotive and neuromuscular abnormalities originate from muscular defects since MIM is not expressed in adult skeletal muscle (Mattila et al., 2003), and no gross morphological or histological defects were detected in $MIM^{-/-}$ skeletal muscle (data not shown).

From the data presented above, the clearest example linking MIM deficiency to behavioral defects was the cerebellum, as we found that MIM is highly expressed in Purkinje neurons (Figure 2), required for normal spine density of Purkinje cells (Figures 3A-3C) and was important for the maintenance of motor coordination functions (Figure 4I), which essentially depend on Purkinje cells. To investigate the synaptic inputs in Purkinje cells of MIM^{+/+} and MIM^{-/-} mice, we used whole-cell patch-clamp technique to record spontaneous miniature excitatory and inhibitory post-synaptic currents (mEPSC and mIPSCs) in the somatic area (Figure 4L). Strikingly, we found that the mEPSC frequency was lower in $MIM^{-/-}$ (0.58 ± 0.10 Hz) as compared with $MIM^{+/+}$ Purkinje neurons (0.94 \pm 0.11 Hz, p < 0.05, N = 6 per genotype in all recordings) (Figure 4M), with no significant differences in the mEPSC amplitudes (Figure 4N) or decay times (MIM+/+: 25.14 ± 6.17 pA and 9.52 ± 0.16 ms; $MIM^{-/-}$: 23.29 ± 5.60 pA and 9.96 ± 0.35 ms, NS). Importantly, no differences were detected between the MIM +/+ and MIM-/- mice in mIPSC frequency ($MIM^{+/+}$, 0.45 ± 0.16 Hz; $MIM^{-/-}$, 0.57 ± 0.11 Hz. NS) or mIPSC amplitudes or decay times ($MIM^{+/+}$: 19.64 ± 8.05 pA; $15.1 \pm 0.29 \text{ ms}$; $MIM^{-/-}$: $20.25 \pm 9.73 \text{ pA}$; $15.9 \pm 0.17 \text{ ms}$, NS),

(K) MIM-deficient mice are more sensitive to a thermal stimulus. The hot-plate test revealed a hyperalgesic phenotype in MIM mutants, which responded to the thermal stimulus significantly faster than the WT littermates. Young (10-13 week) mice, n = 20 mice per genotype (10 males, 10 females), and aged (44-45 weeks) mice, n = 10 mice per genotype (5 males, 5 females).

(L-N) Spontaneous miniature postsynaptic currents (mPSCs) in Purkinje neurons from WT and MIM-/- mice. (L) Representative traces of spontaneous mEPSCs and mIPSCs in MIM+/+ and MIM-/- Purkinje neurons from cerebellar lobe VIII. mEPSCs are seen as inward currents (downward deflections), and mIPSCs are seen as outward currents (upward deflections). The traces in expanded timescale show average of ten events from each recording. There were no differences in amplitudes or decay times of the mEPSCs or mIPSCs between the genotypes. (M) The frequency of mEPSCs was significantly higher in MIM++ mice compared with MIM^{-/-} mice. (N) There were no differences in the frequency of mIPSCs between the genotypes. Data are represented as mean ± SEM, *p < 0.05, **p < 0.01, ***p < 0.001.







respectively. In summary, these recordings demonstrate that MIM-deficient mice display decreased synaptic excitation/inhibition ratio in Purkinje neurons, correlating with the observed expression and morphological defects in the Purkinje neurons and the dysfunctional motor coordination of MIM-deficient mice.

Direct I-BAR-Driven Membrane Bending Is the Underlying Mechanism behind MIM-Mediated Spine Nucleation

The evidence above proposed that MIM-mediated spine initiation plays an important role for brain function. To understand the mechanistic basis of spine initiation by MIM, we took advantage of different loss of function MIM mutant alleles (Figure 5). MIM has been described to have several biochemical activities, such as actin monomer binding (Mattila et al., 2003), Rac1 GTPase binding (Bompard et al., 2005; Mattila et al., 2007), membrane (PIP) binding/bending (Mattila et al., 2007; Suetsugu et al., 2006; Saarikangas et al., 2009), and membrane insertion/ curvature sensing activities (Saarikangas et al., 2009; Maddugoda et al., 2011). In NIH 3T3 fibroblasts, exogenous expression of full-length MIM resulted in the formation of membrane extensions such as ruffles and filopodia, and this activity is preserved to a minimal region in the N terminus corresponding to the membrane bending I-BAR domain (Figures 5A-5C). To analyze whether the membrane-bending and actin-binding activities contribute to spine initiation by MIM in neurons, we first transfected rat hippocampal neurons with GFP-tagged MIM constructs, which display specific defects either in membrane PIP binding (Figure 5D; Mattila et al., 2007) or in actin binding (Figure 5E; Mattila et al., 2003) (structures from Lee et al., 2007). Interestingly, whereas the actin-binding mutant potentiated spine formation similarly to WT MIM (see Figure 1F), the membrane-binding-deficient mutant was unable to do so (Figures 5F-5I and 5L). In fact, expression of the membrane-binding-deficient mutant resulted in decreased spine density as compared with GFP transfected neurons, suggesting that due to the dimeric nature of MIM (Lee et al., 2007), it might function as a dominant-negative construct that sequesters endogenous MIM into non-functional hetero-oligomers. To further investigate the mechanism by which the I-BAR domain promotes spine formation, we compared spine densities between neurons transfected with I-BAR domain alone (minimal region with membrane deforming activity) and I-BAR domain mutant that lacks membrane inserting and positive membrane curvature sensing N-terminal amphipathic alpha helix (Saarikangas et al., 2009; Maddugoda et al., 2011) (Figures 5J, 5K, and 5M). Importantly, whereas the I-BAR alone was capable of potentiating spine filopodia formation, the insertion mutant could not drive spine formation (Figure 5M), suggesting that both PIP-binding and curvaturesensing abilities of the I-BAR domain contribute to spine initiation. Importantly, we could also rescue the decreased spine density phenotype of MIM^{-/-} neurons with MIM-GFP and MIM I-BAR constructs, but not with the membrane-binding-deficient mutant (Figure S3A), altogether showing that the membrane bending activity is crucial for MIM-induced spine morphogenesis.

Extended morphological characterization of spines in neurons mildly overexpressing MIM revealed several signatures of MIM action in spine morphogenesis: MIM overexpression decreased spine length and width (Figures 5N and 5O), which is seen by significantly more pronounced existence of thin (Figure 5P) and stubby spines (Figure 5Q), whereas the amount of mushroom shaped spines was significantly decreased in MIM overexpressing neurons (Figure 5R). These data are in agreement with the alterations found in MIM-deficient neurons, which displayed decreased number of total, and especially thin spines, as well as increased head width (Figures 3F, 3G, and 3I).

The reduced number of mushroom spines suggested that MIM might restrict spine head expansion associated with maturation. Hence, we tested whether MIM overexpression-induced dendritic filopodia or thin spines can undergo transition into mushroom spines. To this end, we imaged hippocampal neurons expressing GFP or MIM-GFP and measured the rate of protrusion initiation and the rate of conversion from filopodia to mushroom spine. Importantly, mild MIM overexpression resulted in a 2-fold increase in the initiation rate of protrusions as compared with GFP control (237 versus 119 initiations/m of dendrite/hr, $N_{(MIM)}$ = 108 and $N_{(GFP)}$ = 55; data not shown). However, the portion of filopodia that underwent head expansion (maturation) was greatly reduced in MIM-overexpressing cells as compared with GFP-expressing cells (28 versus 13 maturations/m of dendrite/hr, $N_{(MIM)} = 6$ and $N_{(GFP)} = 13$; data not shown).

Figure 5. MIM Promotes Dendritic Spine Morphogenesis through Its Membrane Bending I-BAR Domain

(A-C) NIH 3T3 fibroblasts transfected with GFP, full-length MIM, or MIM I-BAR domain. The membrane-deforming activity resides in the N-terminal I-BAR domain, which deforms the plasma membrane into filopodia-like tubules.

(D) Structure of MIM membrane bending I-BAR domain (Protein Data Bank [PDB]: 2D1L; Lee et al., 2007). The lysine residues responsible for membrane binding/ bending (K146, K149, K150) are colored gray and the membrane inserting N terminus is colored in lime. The dashed line indicates the membrane-binding interface

(E) MIM actin monomer-binding WH2 domain (orange) bound to actin (gray) (PDB: 2D1K, Lee et al., 2007). Lime indicates the mutated residues (K746,747A) and the deleted part 749-759 in the actin-binding-deficient MIM construct.

(F-K) Representative images of DIV 14 rat hippocampal neurons transfected with mCherry in combination with (F) GFP control, (G) MIM full-length-GFP, (H) MIM no-membrane binding mutant, (I) MIM no-actin binding mutant, (J) MIM-I-BAR domain, and (K) MIM-I-BAR domain without the N-terminal membrane insertion

(L) As compared with GFP-expressing neurons, MIM potentiates spine formation (p < 0.05; see Figure 1E), for which actin binding is not required (p < 0.05), but the membrane binding is essential (NS).

(M) The minimal region with the membrane deforming activity (I-BAR) is sufficient to potentiate spine formation, but requires the membrane inserting N-terminal

(N and O) MIM overexpression results in decreased spine length (p < 0.01).

(P-R) Overexpression of MIM increases the amount of thin (p < 0.05) and stubby spines (p < 0.001) and results in an overall reduction of mushroom shaped spines (p < 0.05)

Data are represented as mean \pm SEM. Scale bars represent 5 μm . See also Figure S3.



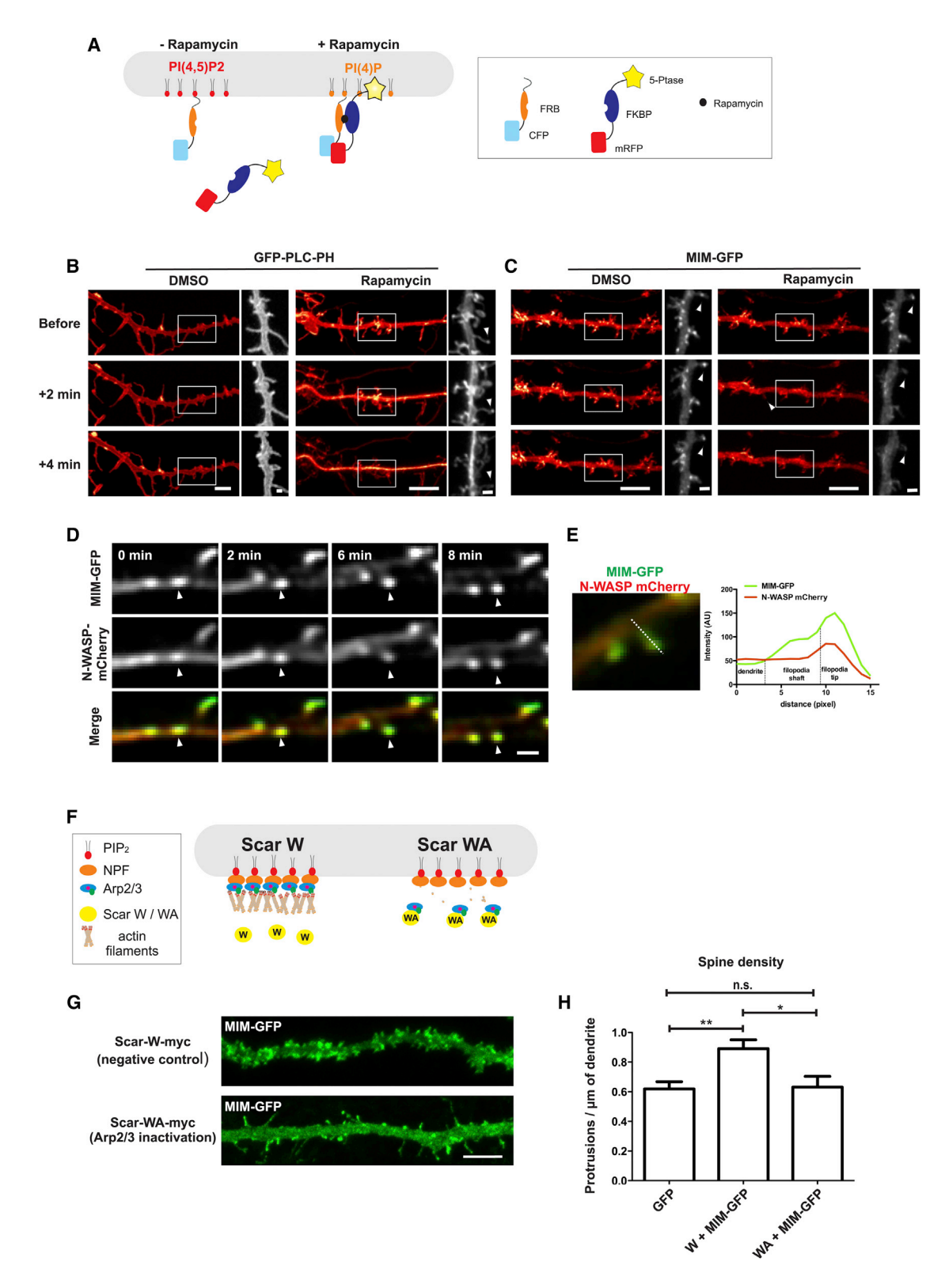


Figure 6. MIM Is Recruited to the Plasma Membrane by PIP Signaling and Requires Arp2/3-Actin Assembly to Promote Spine Formation (A) Schematic representation of the PI(4,5)P2 depletion system (Varnai et al., 2006). Addition of rapamycin dimerizes the FRB and FKBP domains and brings the 5-ptase enzyme to the plasma membrane, where it dephosphorylates PI(4,5)P2 at the 5' position. (B) DMSO treatment has no effect on GFP-tagged PLC-PH domain, which binds PI(4,5)P2 specifically, whereas addition of rapamycin results in rapid trans-

location of PH-domain to the cytoplasm (arrowheads).



Furthermore, when we analyzed the number of spines that displayed postsynaptic density (SAP97-mCherry) as a sign of spine maturation, we found that MIM overexpressing cells displayed 29% reduction in the density of PSD-containing spines as compared with the GFP control cells (0.17 PSDs per µm versus 0.24 PSDs per μ m, $N_{(MIM)}$ = 106 and $N_{(GFP)}$ = 135, respectively; Figure S3B), which is in agreement with the reduction of mushroom spines in MIM overexpressing cells (Figure 5R). Although these data suggest that MIM does hinder spine head expansion, we were unable to detect events where MIM signal would disappear during spine maturation in our live-cell experiments (data not shown). However, analysis of anti-MIM antibody-labeled neurons indicated that MIM is not enriched in all mushroom spines. Taken together, these data suggest that both MIM activity and its localization are likely to be regulated during spine maturation. Altogether, these data demonstrate two important aspects: (1) spine initiation is driven by I-BAR domain-mediated membrane deformation, and (2) MIM assembly at the tip of thin spines (Figure 1C) restricts dendritic spine maturation.

PIPs Are Critical for MIM-Plasma Membrane Interaction

The signaling pathways potentiating spine filopodia formation are poorly understood. However, recent data suggest a central role for phosphorylated PIPs in spine morphogenesis. For example, brain-derived neurotrophic factor (BDNF) stimulated filopodia initiation by promoting PI3-kinase signaling and accumulation of PI(3,4,5)P₃ to dendritic filopodia (Luikart et al., 2008), and spines were found to be enriched in PI(4,5)P2 (Horne and Dell'Acqua 2007). We have previously shown that the positively charged poles of I-BAR domain of MIM bind to PIPs (Mattila et al., 2007), but it is not known whether PIPs are directly involved in MIM recruitment/function in cells. Since membrane binding was essential for MIM-mediated spine initiation (Figures 5H and 5K-5M), we hypothesized that PIP-signaling might be responsible for MIM recruitment and proto-protrusion assembly. To test whether PIPs, in particular PI(4,5)P₂ and/or PI(3,4,5)P₃, are required to recruit and maintain MIM-plasma membrane interactions in neurons, we utilized the inducible PI5P-depletion system, which encompasses two constructs: a plasma membrane bound CFP-tagged FRB domain and a cytosolic mRFPtagged FKBP12 fused to a 5-phosphatase (5-ptase) domain that catalyzes conversion of PI(4,5)P2 (PIP2) into PI(4)P and PI(3,4,5)P₃ (PIP3) into PI(3,4)P₂ (Varnai et al., 2006; Figure 6A). FRB and FKBP dimerize upon addition of rapamycin into the culture medium, which brings the 5-ptase-FKBP chimera to the plasma membrane to dephosphorylate the inositide ring at the 5' position (Figure 6A). To control the assay, we used PIP2-specific plecstrin homology (PH) domain of phospholipase C (PLC) fused to a GFP. As expected, the addition of rapamycin resulted in a rapid loss of PH-domain from the plasma membrane (see arrowhead in Figure 6B), whereas DMSO-control had no effect (Figure 6B). By examining cells expressing MIM-GFP and PIP2/ PIP3-depletion constructs, we found that addition of rapamycin, but not DMSO control, resulted in a rapid relocalization of MIM from the plasma membrane and tips of filopodia to the cytoplasm (compare arrowheads in Figure 6C). This was particularly evident in MIM-enriched proto-protrusions, from where MIM vanished rapidly after rapamycin addition. These data demonstrate that PIP2/PIP3 signaling is an important upstream regulator for the membrane recruitment of MIM and in good agreement with the data demonstrating that the PIP-binding interface of MIM is critical for its function in spine initiation (Figures 5H and 5L).

Arp2/3 Complex-Mediated Actin Assembly Is Required for MIM-Induced Spine Formation

We next aimed to identify the pathways downstream of the PIP-MIM axis that are responsible for actin assembly and spine elongation (Figure 11). Because PIP2/PIP3 are known to have positive effects on actin assembly (Saarikangas et al., 2010) and MIM I-BAR domain, like all BAR domains, promotes the formation of PIP2-enriched domains on membranes (Saarikangas et al., 2009; Zhao et al., 2013), we hypothesized that PIP-responsive actin regulators might be co-recruited to spine filopodia together with MIM. To test this, we co-expressed MIM-GFP together with Neuronal-WASP (N-WASP) in hippocampal neurons and dissected their temporal recruitment to the future spine filopodia. N-WASP is an actin nucleation-promoting factor (NPF) that binds to and is sharply activated by small increase in PIP2 density to promote Arp2/3 complex-mediated actin polymerization (Papayannopoulos et al., 2005). Live neuron microscopy analysis of initiating filopodia showed that N-WASP localized to protoprotrusions and launching filopodia together with MIM (arrowheads in Figure 6D; N = 21). A more detailed line-scan analysis of maturing spine suggested that N-WASP localization might be more restricted to the head where the actin assembly takes place, while MIM, in addition to head enrichment, is also found along the shaft (Figure 6E).

N-WASP is an activator of the actin-nucleating Arp2/3 complex. In order to test whether Arp2/3-mediated actin assembly is required for MIM induced proto-protrusion elongation, we co-expressed MIM-GFP together with Scar WA-myc construct, which encodes a truncated Scar protein that sequesters Arp2/3 complex from the nucleation promoting factors such as N-WASP keeping it misplaced and inactive. As a negative control, we used Scar-W construct that does not bind Arp2/3 complex (Machesky and Insall 1998; Figure 6F). Quantification of spine density in MIM-GFP/WA-co-expressing cells (Figure 6G) demonstrated that Arp2/3 activity is critical for MIM function in potentiating spine formation (Figures 6G and 6H; p < 0.05).

⁽C) Addition of rapamycin, but not DMSO, induces rapid re-localization of MIM from the plasma membrane into the cytoplasm (arrowheads in magnified regions).

⁽D) Live-cell imaging on neurons co-expressing MIM-GFP and N-WASP-mCherry during proto-protrusion and spine filopodia formation.

⁽E) Line-scan analysis of N-WASP-mCherry and MIM-GFP intensities in spine filopodia.

⁽F) Schematic representation of the Arp2/3 inactivation system: the ectopic expression of Scar WA region sequesters Arp2/3 from its native location and prevents its activation.

⁽G) Representative images of cells expressing MIM-GFP together with Scar WA or W.

⁽H) Quantification of spine density in cells expressing MIM-GFP together with Scar W or WA constructs. *p < 0.05, **p < 0.01.

Data are represented as mean ± SEM. Scale bars represent 5 µm (B, C, and F), 1 µm (right in B and C), and 2 µm (D).



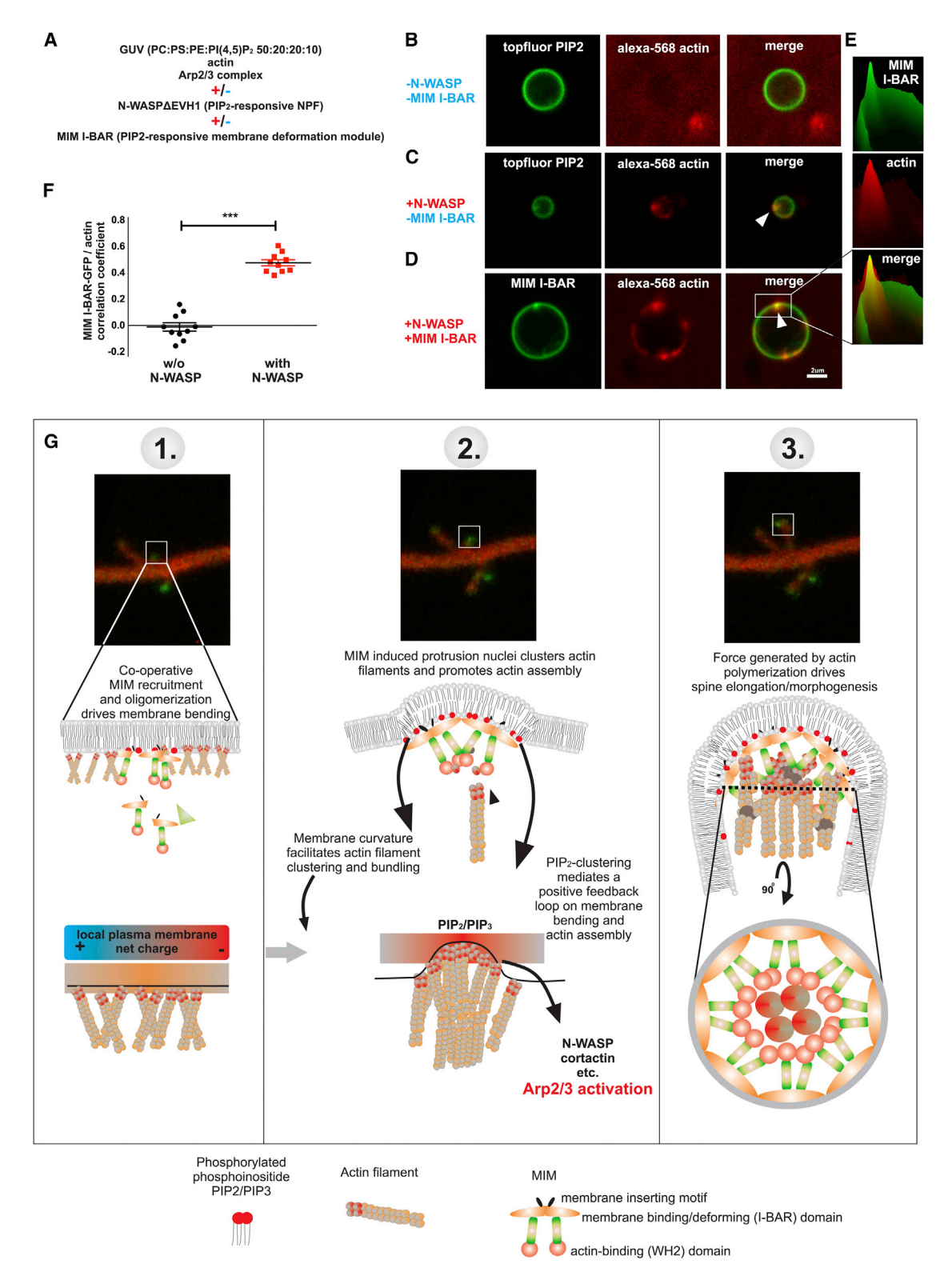


Figure 7. MIM I-BAR and PIP2-Responsive Arp2/3 Actin Assembly Co-organize on PIP2-Rich Vesicles

- (A) The synthetic approach combining GUVs actin, Arp2/3 together with N-WASP and/or MIM I-BAR-GFP.
- (B) Representative image of a GUV (topfluor PIP2, green) and Alexa-568-labeled actin (red) in the absence of N-WASP or MIM-I-BAR.
- (C) Addition of N-WASP directs actin (red) to the GUV surface (green) where it forms foci that coincide with PIP2 foci (arrowhead).



Co-expression of Scar-WA domain with MIM prevented the MIM-induced increase in spine density, while the proto-protrusions were still able to assemble (Figures 6G and 6H). Collectively, these analyses propose that PIP (PIP2/PIP3) signaling acts as an upstream factor to recruit MIM to the plasma membrane, and this might be coupled to the recruitment and local activation of PIP-responsive Arp2/3-dependent actin assembly machinery to drive the protrusion elongation.

Reconstituted I-BAR-Mediated Membrane Bending and Arp2/3-Actin Assembly Machineries Coincide on Model Membranes in a PIP2-Dependent Manner

We have previously shown that MIM I-BAR domain self-organizes on giant unilamellar vesicles (GUVs) into PIP2-rich foci at the sites of membrane deformation (Saarikangas et al., 2009). To examine whether PIPs alone are sufficient to recruit and initiate the self-organization of both MIM-mediated membrane bending and Arp2/3-mediated actin assembly machineries at model membranes, we undertook a minimal synthetic reconstruction approach composed of PIP2-containing GUVs, fluorescently labeled actin, Arp2/3 complex, N-WASP, and MIM I-BAR-GFP (Figure 7A). First, we imaged fluorescently labeled GUVs and actin mixed with Arp2/3 complex. As expected, no actin assembly or recruitment was detected on the GUV surface in the absence of Arp2/3 activator (Figure 7B). Importantly, addition of N-WASP was sufficient to localize actin assembly to the GUV surface, in agreement with N-WASP being recruited and activated at the membrane via its polybasic domain-PIP2 interaction (Figure 7C; Papayannopoulos et al., 2005). Interestingly, similarly to BAR domain scaffolds (Saarikangas et al., 2009; Zhao et al., 2013), we found that these actin assembly foci displayed higher PIP2 density as compared with the neighboring regions on the GUV (arrowhead in Figure 7C), suggesting that the polybasic domain of N-WASP alone might be sufficient to cluster PIP2 and thereby promote self-organization/activation of actin assembly at membranes. Finally, since both the membrane bending and actin assembly machineries are PIP2-responsive, we tested how these machineries are spatially organized relative to each other. We thus added GFPtagged MIM I-BAR domain (minimal region capable of membrane bending) to GUVs containing the PIP2-responsive actin assembly machinery (Figure 7D). This resulted in self-assembly of MIM I-BAR-GFP and PIP2-responsive actin assembly machinery at the same foci on the membrane (arrowhead in Figure 7D). Surface plot of this region demonstrated how polymerized actin spanned away from the membrane, whereas MIM was only present at the membrane (Figure 7E). Thus, MIM does not incorporate into the actin filaments, but is instead recruited to the foci via PIP2 binding (Saarikangas et al., 2009). We quantified the correlation co-efficient between actin and MIM-I-BAR on GUVs in the presence or absence of N-WASP. In the presence of N-WASP, the correlation co-efficient value between MIM and actin was 0.47, whereas in the absence of N-WASP it was -0.01 (1 represents perfect, 0 no, and -1 perfect inverse colocalization) (Figure 7F; p < 0.001, n = 10 per group), altogether demonstrating that regions of high MIM I-BAR intensity coincide with regions of PIP2-responsive actin assembly on membranes. Collectively, these data provide evidence that PIP2 is sufficient to initiate the formation of spatially restricted, self-organizing domains of protrusive activity by polarizing two distinct but intercommunicative morphogenetic pathways: the I-BAR-driven membrane bending and the actin-dependent force-generating machinery.

DISCUSSION

The actin cytoskeleton and many of its regulators have been shown to play a pivotal role in dendritic spine morphogenesis (Hotulainen and Hoogenraad, 2010; Svitkina et al., 2010). However, the molecular underpinnings that prime actin assembly to determine where and how spine protrusions are initiated have remained obscure. Here we provide evidence that membranesculpting proteins might be universal factors to initiate the formation of proto-protrusions, which function as launching pads for actin assembly. We show that I-BAR protein MIM nucleates spine formation through its membrane deforming activity, which occurs independently and prior to actin assembly. MIM is recruited to the plasma membrane by PIPs that provide a bimodal signal for protrusion formation by activating both the membrane bending activity of MIM and by stimulating actin polymerization. Indeed, we found that Arp2/3 complex-dependent actin polymerization was necessary for MIM-potentiated protrusion elongation. In neurons, MIM was enriched in dendrites, especially in proto-protrusions, dendritic filopodia, and spines. Loss of MIM resulted in decreased number of spines in vivo and in vitro with characteristic alterations in spine morphology, most notably a loss of thin spines, which are the precursor structures for more mature spine types. Consequently, MIM-deficient mice displayed attenuated synaptic transmission and a wide spectrum of behavioral defects, underscoring the necessity of MIM-driven neuronal morphogenesis for proper CNS function.

PIPs as Organizers of Protrusion Initiation

From the obtained data, we propose the following model to explain how MIM imposes its function during spine formation (see Figure 7G): neuronal growth factors such as BDNF promote

⁽D) Addition of MIM-I-BAR-GFP results in MIM I-BAR enriched clusters and membrane invaginations, which co-inside with foci of actin assembly (see arrowhead in D).

⁽E) Surface plot of actin and MIM I-BAR intensities at the indicated regions in (D).

⁽F) Quantification of correlation co-efficient between actin and MIM I-BAR GFP in samples with or without N-WASP, demonstrating that actin localizes to the membrane in the presence of N-WASP, and the regions of high MIM I-BAR-GFP intensity are overlapping the region of high actin intensity. Data are represented as mean ± SEM.

⁽G) Model how MIM initiates dendritic spine formation. (1) MIM responds to local PIP synthesis at the plasma membrane. The initial recruitment results in dimerization, co-operative self-assembly, and activation of the membrane-deforming activity. The dynamic MIM oligomerization promotes PIP-rich lipid domain formation at the membrane. (2) The resulting MIM-initiated proto-protrusion recruits PIP2/PIP3-responsive actin modulators such as N-WASP to promote actin assembly. The membrane bending by MIM clusters underlying sub-membranous actin filament barbed ends together to form a weak bundle. (3) Resulting actin assembly drives the elongation and morphogenesis of the dendritic spine.



PIP signaling (Luikart et al., 2008), resulting in local increase in negative charge at the plasma membrane. This recruits MIM via its positively charged poles of the I-BAR domain, induces its dimerization, and activates its membrane bending activity. The resulting curvature and simultaneous clustering of PIPs (by preventing their free diffusion) promote co-operative oligomerization of MIM, ultimately resulting in the induction of outward membrane curvature. We propose that this membrane bending step in protrusion formation functions to overcome the very first energetically unfavorable membrane deformation step in protrusion formation.

Importantly, MIM interacts dynamically with membranes in protrusions (Saarikangas et al., 2009), which would allow competitive recruitment/activation of other PIP responsive molecules. These PIP2/PIP3-responsive actin regulators that function in spinogenesis include, e.g., N-WASP (Papayannopoulos et al., 2005), formin mDia2 (Hotulainen et al., 2009; Gorelik et al., 2011), and GTPases such as Rac (Heo et al., 2006), which all bind to negatively charged membranes dynamically via large positively charged interfaces (Papayannopoulos et al., 2005; Heo et al., 2006). Therefore, these molecules are also expected to restrict the diffusion of PIPs from the spine initiation site, which can be further boosted by the low-affinity multivalent proteinprotein interactions among these proteins (Li et al., 2012). We propose that this phenomena might generate a self-organizing "protrusion hub" that responds to shallow increase in local PIP density, slows down lipid diffusion, and thereby generates a self-amplifying positive feedback loop that promotes membrane deformation and actin assembly. Importantly, we were able to reconstruct the self-organizing aspects of the PIP-responsive protrusion hub in vitro by combining a minimal set of components: PIP2-containing GUVs, PIP2-responsive actin assembly machinery (actin, N-WASP, and Arp2/3), and PIP2-responsive membrane-bending I-BAR domain of MIM. Here, PIP2 was sufficient to self-organize and co-cluster the two independent machineries (membrane bending and actin assembly) into a single zone of activity at the membrane. Collectively, such selforganizing system might help establish spatial control for protrusion formation in response to local activation of PIP signaling.

From a geometrical stand point, it is interesting to note that by bending the plasma membrane into a tube (Figure 7G), MIMmediated membrane bending could also direct pre-existing and newly assembled sub-membranous actin filaments to fuel spine elongation. In vitro, branched actin filaments growing against membranes get clustered and weakly bundled by the surrounding membrane (Liu et al., 2008). Furthermore, actin filaments nucleated on V-shaped micropatterns form parallel filopodia-like bundles even in the absence of bundling proteins and surrounding membrane (Reymann et al., 2010). Thus, we propose that MIM-induced membrane protrusion might direct and cluster branched actin filaments to form a weak bundle. This is in agreement with the actin filament organization found in dendritic filopodia, spine necks, and I-BAR domain-induced filopodia (Korobova and Svitkina, 2010; Yang et al., 2009).

I-BAR and IF-BAR Proteins May Be Generic Protrusion Initiators

Although spine density was lower in MIM-deficient mice, dendritic protrusions still formed, which indicates that MIM-independent mechanisms of spine initiation must exist. It is likely that

there is redundancy between I-BAR/IF-BAR family members during spinogenesis. There are five I-BAR domain and several IF-BAR proteins in mammals (Zhao et al., 2011; Coutinho-Budd et al., 2012), many of which are expressed in the CNS and described to have a role in dendritic spine morphogenesis (Choi et al., 2005; Kim et al., 2009; Sawallisch et al., 2009; Carlson et al., 2011; Charrier et al., 2012). Interestingly, similar to MIM, IF-BAR containing WRP/SRGAP3 has been indicated to play a role in spine initiation (Carlson et al., 2011). Hence, it is plausible that the membrane curvature-driven spine/filopodia initiation is a general mechanism to drive the formation of a distinct subset of cell protrusions within and outside the CNS. Different I-BAR/F-BAR proteins might be specified through alternative expression programs or by having different upstream regulation and/or downstream effectors, resulting in different types of filopodia/spines in different cell types at a given stage of development. This would explain the different behavioral phenotypes observed in WRP/ SRGAP3 (Carlson et al., 2011) and MIM knockout mice. It is also important to note that in addition to its role in spine initiation, MIM also had a restrictive role in spine head expansion. While we did not observe GFP-MIM removal during spine maturation, the endogenous MIM was found localized in a minority of mushroom spine heads. Thus, it is plausible that MIM activity and/or localization are regulated during spine maturation.

Behavioral analysis revealed several effects of MIM deficiency (Figure 4). In particular, the defect in motor coordination is likely to be linked to decreased spine density and attenuated excitatory synaptic transmission in the cerebellum in the MIM mutants (see Figures 3 and 4; Huang et al., 2012). The Purkinje neurons are the sole output from the cerebellar cortex to the cerebellar nuclei, which in turn are the main output structure of the cerebellum (Reeber et al., 2013). Thus, decreased excitatory drive in association with no differences in the inhibition in Purkinje neurons would result in less powerful output of Purkinje neurons to their target neurons and thus likely lead to motoric dysfunctions (Reeber et al., 2013). Interestingly, deletion of the MIM homolog in Drosophila also resulted in locomotor and motor coordination abnormalities in flies (Quinones et al., 2010), indicating that the function of MIM in neuronal morphogenesis is likely to be conserved in evolution. Dysfunctional I-BAR-like proteins have been linked to disorders such as mental retardation and neurodegeneration (McCrea and De Camilli, 2009; Endris et al., 2002) and shown to be important for corticogenesis (Charrier et al., 2012). Hence, it would be interesting to examine whether these disorders are contributed by disturbances at the level of spine initiation, either by dysfunctional PIP signaling, I-BAR-mediated membrane bending, or improper actin assembly. In an evolutionary scheme, it is thrilling to note that PIP-responsive growth of actin structures against cellular membranes represents a conserved continuum of polarity establishment utilized by fungi, motile amoebas, and metazoans (Saarikangas et al., 2010; Vernay et al., 2012) and, as shown here, culminating in the formation of synaptic structures that form the basis of normal brain functions.

EXPERIMENTAL PROCEDURES

GUV Assays

The preparation of GUVs is described in the Supplemental Experimental Procedures. The GUV experiments were performed as described in (Zhao



et al., 2013), with the following exceptions: GUVs were pre-incubated with His-N-WASP Δ EVH1 for 10 min and then diluted in actin polymerization buffer (10 mM Tris HCl, 2 mM MgCl₂, 100 mM KCl, 1 mM ATP, 1 mM DTT [pH 7.5]) containing 200 mM sucrose, actin, and Arp2/3 complex. The protein concentration in the final mixture was actin (4.7 μ M), Arp2/3 complex (111.5 nM), and N-WASP (0.5 μ M). MIM I-BAR was added to the GUVs at the concentration of 0.5 μ M.

MIM Mice

The generation of C57BL/6 MIM mutant mice is described in (Saarikangas et al., 2011). Animals were handled in accordance with relevant national and/or local animal welfare bodies, and the appropriate committees approved all animal work. Behavioral analyses have been performed at the German Mouse Clinic (http://www.mouseclinic.de; Gailus-Durner et al., 2009).

Neuronal Cultures, Transfections, and Fixed Sample Preparation

Hippocampal neuronal cultures were prepared as described previously (Bertling et al., 2012). Transient transfections were performed on DIV13 using Lipofectamine 2000 (Invitrogen) as described in Hotulainen et al. (2009). The neurons were fixed with 4% formaldehyde. Proteins were visualized by immunofluorescence staining as follows: the myc-tagged Scar W and WA constructs, mouse anti-c-Myc antibody (1:200; Sigma-Aldrich), MIM, rabbit polyclonal anti-MTSS1 antibody (1:50; Imgenex).

Image Analysis, Measurements and Spine Density, and Morphology

To assess the density of spines of Purkinje cells, cells of P16 $\emph{MIM}^{+/+}$ and $\emph{MIM}^{-\prime-}$ mice were injected with biocytin, fixed with 4% formaldehyde, and stained with Alexa Fluor 555 Streptavidin Conjugate (Molecular Probes). Slices were imaged with Leica HCS SP5 confocal microscope, using HyD detector, pinhole 60 μm , 63 \times water objective, 12-bit detection, resulting in voxel size $0.08 \times 0.08 \times 0.21 \ \mu m$. All ex vivo images were deconvoluted with AutoQuant software (MediaCybernetics). The spine density was analyzed from 13 MIM+/+ and 15 MIM^{-/-} neurons with NeuronStudio (Rodriguez et al., 2008).

The spine phenotype analysis on transfected neurons was performed with images with a voxel size of 0.078 × 0.078 × 0.122 μm. After modeling of the dendrite surface, protrusions with a minimum volume of 5 voxels (0.020 μm^3), length between 0.2 and 5 μm , and a maximal width of 3 μm were retained as spines. Following the default settings of the NeuronStudio program (Rodriguez et al., 2008), spines with a minimum head diameter of $0.35\,\mu m$ and a minimum head versus neck ratio of 1.1 were classified as mushroom spines. Non-mushroom spines with a minimum volume of 10 voxels (0.040 μm³) were classified as stubby spines. All other spines were considered thin. Image files were processed with LAS-AF (Leica Microsystems), Photoshop CS4 (Adobe), and Image J. The line scans were done with Image J plot profile function. The kymograph analysis was conducted using Image J plugin (http://www.embl.de/eamnet/html/body_kymograph.html), and the resulting kymograph was processed with a Gaussian blur filter. To quantify the colocalization between two images on the GUVs, we calculated Pearson's correlation coefficient using ImageJ plugin. Intensity profiles for the GUVs were generated using the ImageJ surface profile function.

For plasmids, protein expression and purification, western blotting, immunohistochemistry and microscopy, electrophysiology, and mouse behavioral testing, see Supplemental Experimental Procedures.

Statistical Analyses

All the graphs were generated, and the statistical analyses were carried out with Prism 5.0b. The graphs display mean ± SEM, and Student's t test and ANOVA (with Newman-Keuls post hoc test) were used for statistical comparisons.

SUPPLEMENTAL INFORMATION

Supplemental Information includes Supplemental Experimental Procedures and three figures and can be found with this article online at http://dx.doi. org/10.1016/j.devcel.2015.04.014.

ACKNOWLEDGMENTS

We thank Y. Barral, J. Einicke, M. Färberböck, S. Kundt, S. Lågas, O. Nikkilä, V. Paavilainen, Y. Sonntag, R. Seeliger B. Sperling, A. Wohlbier, and H. Zhao, as well as the GMC animal caretaker team and the Light Microscopy Unit at the Institute of Biotechnology, University of Helsinki for support and expert technical assistance. We are grateful to T. Balla, G. Garner, L. Machesky, J. Taunton, M. Vartiainen, and R. Wedlich-Söldner for kindly providing plasmid constructs. This work was supported by GBPM-Training Program, a FEBS Long-Term Fellowship and Finnish Cultural Foundation (to J.S.); the Ministry of Education, Scientific Research and Techniques (to N.K.): Astellas Foundation for Research on Metabolic Disorders and Scandinavia-Japan Sasakawa Foundation (to Y.S.); Academy of Finland (to P.H. [SA 1266351], P.L., and C.R. [SA 259799]); University of Helsinki, University of Aix-Marseille and ANR-13-BSU4-0012-01 (to C.R.); the German Federal Ministry of Education and Research grants to the German Center for Vertigo and Balance Disorders (grant 01 EO 0901), to the German Center for Neurodegenerative Diseases (DZNE), and to the GMC (NGFN-Plus grants 01GS0850, 01GS0851, 01GS0853; Infrafrontier grant 01KX1012); and the Initiative and Networking Fund of the Helmholtz Association in the framework of the Helmholtz Alliance for Mental Research in an Ageing Society (HA-215).

Received: November 22, 2013 Revised: January 28, 2015 Accepted: April 21, 2015 Published: June 4, 2015

REFERENCES

Alvarez, V.A., and Sabatini, B.L. (2007). Anatomical and physiological plasticity of dendritic spines. Annu. Rev. Neurosci. 30, 79-97.

Bertling, E., Ludwig, A., Koskinen, M., and Hotulainen, P. (2012). Methods for three-dimensional analysis of dendritic spine dynamics. Methods Enzymol. 506, 391-406.

Bompard, G., Sharp, S.J., Freiss, G., and Machesky, L.M. (2005). Involvement of Rac in actin cytoskeleton rearrangements induced by MIM-B. J. Cell Sci. 118. 5393-5403.

Bourne, J.N., and Harris, K.M. (2008). Balancing structure and function at hippocampal dendritic spines. Annu. Rev. Neurosci. 31, 47-67.

Carlson, B.R., Lloyd, K.E., Kruszewski, A., Kim, I.H., Rodriguiz, R.M., Heindel, C., Faytell, M., Dudek, S.M., Wetsel, W.C., and Soderling, S.H. (2011). WRP/ srGAP3 facilitates the initiation of spine development by an inverse F-BAR domain, and its loss impairs long-term memory. J. Neurosci. 31, 2447-2460.

Charrier, C., Joshi, K., Coutinho-Budd, J., Kim, J.E., Lambert, N., de Marchena, J., Jin, W.L., Vanderhaeghen, P., Ghosh, A., Sassa, T., and Polleux, F. (2012). Inhibition of SRGAP2 function by its human-specific paralogs induces neoteny during spine maturation. Cell 149, 923-935.

Choi, J., Ko, J., Racz, B., Burette, A., Lee, J.R., Kim, S., Na, M., Lee, H.W., Kim, K., Weinberg, R.J., and Kim, E. (2005). Regulation of dendritic spine morphogenesis by insulin receptor substrate 53, a downstream effector of Rac1 and Cdc42 small GTPases. J. Neurosci. 25, 869-879.

Coutinho-Budd, J., Ghukasyan, V., Zylka, M.J., and Polleux, F. (2012). The F-BAR domains from srGAP1, srGAP2 and srGAP3 regulate membrane deformation differently. J. Cell Sci. 125, 3390-3401.

Dharmalingam, E., Haeckel, A., Pinyol, R., Schwintzer, L., Koch, D., Kessels, M.M., and Qualmann, B. (2009). F-BAR proteins of the syndapin family shape the plasma membrane and are crucial for neuromorphogenesis. J. Neurosci. 29, 13315-13327.

Endris, V., Wogatzky, B., Leimer, U., Bartsch, D., Zatyka, M., Latif, F., Maher, E.R., Tariverdian, G., Kirsch, S., Karch, D., and Rappold, G.A. (2002). The novel Rho-GTPase activating gene MEGAP/ srGAP3 has a putative role in severe mental retardation. Proc. Natl. Acad. Sci. USA 99, 11754-11759.

Gailus-Durner, V., Fuchs, H., Adler, T., Aguilar Pimentel, A., Becker, L., Bolle, I., Calzada-Wack, J., Dalke, C., Ehrhardt, N., Ferwagner, B., et al. (2009). Systemic first-line phenotyping. Methods Mol. Biol. 530, 463-509.



Gorelik, R., Yang, C., Kameswaran, V., Dominguez, R., and Svitkina, T. (2011). Mechanisms of plasma membrane targeting of formin mDia2 through its amino terminal domains. Mol. Biol. Cell 22, 189-201.

Guerrier, S., Coutinho-Budd, J., Sassa, T., Gresset, A., Jordan, N.V., Chen, K., Jin, W.L., Frost, A., and Polleux, F. (2009). The F-BAR domain of srGAP2 induces membrane protrusions required for neuronal migration and morphogenesis. Cell 138, 990-1004.

Hayn-Leichsenring, G., Liebig, C., Miething, A., Schulz, A., Kumar, S., Schwalbe, M., Eiberger, B., and Baader, S.L. (2011). Cellular distribution of metastasis suppressor 1 and the shape of cell bodies are temporarily altered in Engrailed-2 overexpressing cerebellar Purkinje cells. Neuroscience 189, 68-78

Heo, W.D., Inoue, T., Park, W.S., Kim, M.L., Park, B.O., Wandless, T.J., and Meyer, T. (2006). PI(3,4,5)P3 and PI(4,5)P2 lipids target proteins with polybasic clusters to the plasma membrane. Science 314, 1458-1461.

Horne, E.A., and Dell'Acqua, M.L. (2007). Phospholipase C is required for changes in postsynaptic structure and function associated with NMDA receptor-dependent long-term depression. J. Neurosci. 27, 3523-3534.

Hotulainen, P., and Hoogenraad, C.C. (2010). Actin in dendritic spines: connecting dynamics to function. J. Cell Biol. 189, 619-629.

Hotulainen, P., Llano, O., Smirnov, S., Tanhuanpää, K., Faix, J., Rivera, C., and Lappalainen, P. (2009). Defining mechanisms of actin polymerization and depolymerization during dendritic spine morphogenesis. J. Cell Biol. 185,

Huang, T.Y., Lin, L.S., Cho, K.C., Chen, S.J., Kuo, Y.M., Yu, L., Wu, F.S., Chuang, J.I., Chen, H.I., and Jen, C.J. (2012). Chronic treadmill exercise in rats delicately alters the Purkinje cell structure to improve motor performance and toxin resistance in the cerebellum. J. Appl. Physiol. 113, 889-895.

Kim, M.H., Choi, J., Yang, J., Chung, W., Kim, J.H., Paik, S.K., Kim, K., Han, S., Won, H., Bae, Y.S., et al. (2009), Enhanced NMDA receptor-mediated synaptic transmission, enhanced long-term potentiation, and impaired learning and memory in mice lacking IRSp53. J. Neurosci. 29, 1586-1595.

Korobova, F., and Svitkina, T. (2010). Molecular architecture of synaptic actin cytoskeleton in hippocampal neurons reveals a mechanism of dendritic spine morphogenesis. Mol. Biol. Cell 21, 165-176.

Lee, S.H., Kerff, F., Chereau, D., Ferron, F., Klug, A., and Dominguez, R. (2007). Structural basis for the actin-binding function of missing-in-metastasis. Structure 15, 145-155.

Li, P., Banjade, S., Cheng, H.C., Kim, S., Chen, B., Guo, L., Llaguno, M., Hollingsworth, J.V., King, D.S., Banani, S.F., et al. (2012). Phase transitions in the assembly of multivalent signalling proteins. Nature 483, 336-340.

Liu, A.P., Richmond, D.L., Maibaum, L., Pronk, S., Geissler, P.L., and Fletcher, D.A. (2008). Membrane-induced bundling of actin filaments. Nat. Phys. 4,

Luikart, B.W., Zhang, W., Wayman, G.A., Kwon, C.H., Westbrook, G.L., and Parada, L.F. (2008). Neurotrophin-dependent dendritic filopodial motility: a convergence on PI3K signaling. J. Neurosci. 28, 7006-7012.

Machesky, L.M., and Insall, R.H. (1998). Scar1 and the related Wiskott-Aldrich syndrome protein, WASP, regulate the actin cytoskeleton through the Arp2/3 complex. Curr. Biol. 8, 1347-1356.

Maddugoda, M.P., Stefani, C., Gonzalez-Rodriguez, D., Saarikangas, J., Torrino, S., Janel, S., Munro, P., Doye, A., Prodon, F., Aurrand-Lions, M., et al. (2011). cAMP signaling by anthrax edema toxin induces transendothelial cell tunnels, which are resealed by MIM via Arp2/3-driven actin polymerization. Cell Host Microbe 10, 464-474.

Mattila, P.K., Salminen, M., Yamashiro, T., and Lappalainen, P. (2003). Mouse MIM, a tissue-specific regulator of cytoskeletal dynamics, interacts with ATPactin monomers through its C-terminal WH2 domain. J. Biol. Chem. 278, 8452-8459.

Mattila, P.K., Pykäläinen, A., Saarikangas, J., Paavilainen, V.O., Vihinen, H., Jokitalo, E., and Lappalainen, P. (2007). Missing-in-metastasis and IRSp53 deform PI(4,5)P2-rich membranes by an inverse BAR domain-like mechanism. J. Cell Biol. 176, 953-964.

McCrea, H.J., and De Camilli, P. (2009). Mutations in phosphoinositide metabolizing enzymes and human disease. Physiology (Bethesda) 24, 8-16.

Papayannopoulos, V., Co, C., Prehoda, K.E., Snapper, S., Taunton, J., and Lim, W.A. (2005). A polybasic motif allows N-WASP to act as a sensor of PIP(2) density. Mol. Cell 17, 181-191.

Quinones, G.A., Jin, J., and Oro, A.E. (2010). I-BAR protein antagonism of endocytosis mediates directional sensing during guided cell migration. J. Cell Biol. 189, 353-367.

Reeber, S.L., Otis, T.S., and Sillitoe, R.V. (2013). New roles for the cerebellum in health and disease. Front. Syst. Neurosci. 7, 83.

Reymann, A.C., Martiel, J.L., Cambier, T., Blanchoin, L., Boujemaa-Paterski, R., and Théry, M. (2010). Nucleation geometry governs ordered actin networks structures. Nat. Mater. 9, 827-832.

Rodriguez, A., Ehlenberger, D.B., Dickstein, D.L., Hof, P.R., and Wearne, S.L. (2008). Automated three-dimensional detection and shape classification of dendritic spines from fluorescence microscopy images. PLoS One 3, e1997.

Saarikangas, J., Zhao, H., Pykäläinen, A., Laurinmäki, P., Mattila, P.K., Kinnunen, P.K., Butcher, S.J., and Lappalainen, P. (2009). Molecular mechanisms of membrane deformation by I-BAR domain proteins. Curr. Biol. 19,

Saarikangas, J., Zhao, H., and Lappalainen, P. (2010). Regulation of the actin cytoskeleton-plasma membrane interplay by phosphoinositides. Physiol. Rev. 90. 259-289.

Saarikangas, J., Mattila, P.K., Varjosalo, M., Bovellan, M., Hakanen, J., Calzada-Wack, J., Tost, M., Jennen, L., Rathkolb, B., Hans, W., et al. (2011). Missing-in-metastasis MIM/MTSS1 promotes actin assembly at intercellular junctions and is required for integrity of kidney epithelia. J. Cell Sci. 124, 1245-1255.

Sawallisch, C., Berhörster, K., Disanza, A., Mantoani, S., Kintscher, M., Stoenica, L., Dityatev, A., Sieber, S., Kindler, S., Morellini, F., et al. (2009). The insulin receptor substrate of 53 kDa (IRSp53) limits hippocampal synaptic plasticity. J. Biol. Chem. 284, 9225-9236.

Suetsugu, S., Murayama, K., Sakamoto, A., Hanawa-Suetsugu, K., Seto, A., Oikawa, T., Mishima, C., Shirouzu, M., Takenawa, T., and Yokoyama, S. (2006). The RAC binding domain/IRSp53-MIM homology domain of IRSp53 induces RAC-dependent membrane deformation. J. Biol. Chem. 281, 35347-35358.

Svitkina, T., Lin, W.H., Webb, D.J., Yasuda, R., Wayman, G.A., Van Aelst, L., and Soderling, S.H. (2010). Regulation of the postsynaptic cytoskeleton: roles in development, plasticity, and disorders. J. Neurosci. 30, 14937-14942.

Varnai, P., Thyagarajan, B., Rohacs, T., and Balla, T. (2006). Rapidly inducible changes in phosphatidylinositol 4,5-bisphosphate levels influence multiple regulatory functions of the lipid in intact living cells. J. Cell Biol. 175, 377–382.

Vernay, A., Schaub, S., Guillas, I., Bassilana, M., and Arkowitz, R.A. (2012). A steep phosphoinositide bis-phosphate gradient forms during fungal filamentous growth. J. Cell Biol. 198, 711-730.

Yang, C., Hoelzle, M., Disanza, A., Scita, G., and Svitkina, T. (2009). Coordination of membrane and actin cytoskeleton dynamics during filopodia protrusion. PLoS ONE 4. e5678.

Yu, D., Zhan, X.H., Zhao, X.F., Williams, M.S., Carey, G.B., Smith, E., Scott, D., Zhu, J., Guo, Y., Cherukuri, S., et al. (2012). Mice deficient in MIM expression are predisposed to lymphomagenesis. Oncogene 31, 3561-3568.

Zhao, H., Pykäläinen, A., and Lappalainen, P. (2011). I-BAR domain proteins: linking actin and plasma membrane dynamics. Curr. Opin. Cell Biol. 23, 14-21.

Zhao, H., Michelot, A., Koskela, E.V., Tkach, V., Stamou, D., Drubin, D.G., and Lappalainen, P. (2013). Membrane-sculpting BAR domains generate stable lipid microdomains. Cell Rep. 4, 1213-1223.